Article:
Gao, S P, Jiang, J, Cao, M H et al. (2 more authors) (2004) Unoccupied electronic states in CaB6 studied by density functional theory and EELS measurements. Physical Review B. 214419. -. ISSN 2469-9969

https://doi.org/10.1103/PhysRevB.69.214419

Unoccupied electronic states in CaB_6 studied by density functional theory and EELS measurements

Shang-Peng Gao, Jun Jiang, Minghe Cao, Jing Zhu, and Jun Yuan*
Department of Materials Science and Engineering, Tsinghua University, Beijing 100084, People's Republic of China
(Received 7 October 2003; revised manuscript received 25 March 2004; published 22 June 2004)

The electronic structure of CaB_6 has recently attracted great interest because of the discovery that this compound is unexpectedly ferromagnetic and exhibits a surprisingly large thermoelectric effect. We have concentrated on studying the unoccupied electronic states by investigating the boron 1*s* core-level spectroscopy. Comparison of our data from electron energy-loss spectroscopy with that from x-ray absorption spectroscopy using the total electron yield mode reveals evidence for sample inhomogeneity. The *ab initio* band structural method has been successfully applied to simulate the overall features found in the boron 1*s* absorption spectrum. Correlation with the results of a ground state energy-band calculation allows the interpretation of the spectral features in terms of the density of states of the unoccupied conduction band, in particular the identification of a feature associated with hybridization of Ca *d* orbitals with B *p* orbitals. This interpretation is confirmed by comparison with similar calculations for related boride systems. However, simulation spectral data cannot be reconciled with high-resolution experimental data at the absorption threshold. The possibility of either the failure of the theoretical method employed to account for many-body effects and/or the need for improved experimental measurements is discussed.

DOI: 10.1103/PhysRevB.69.214419 PACS number(s): 75.50.Dd, 71.20.−b, 78.20.Bh

I. INTRODUCTION

CaB_6 consists of a three dimensionally interconnected boron atom octahedron (B_6) network, where each octahedron is stabilized by two extra electrons provided by the Ca atoms occupying the interstitial sites in the boron network. It is an important industrial material and has recently attracted a lot of interest because of the discovery that this compound exhibits weak high-temperature ferromagnetism[1] when doped by La, a trivalent rare earth element. Similar magnetic effects have also been detected in La-doped SrB_6 and BaB_6[1]. In addition, it has been found that the Ca-deficient variant $Ca_{1-\delta}B_6$ is also ferromagnetic.[2] In all these compounds, no conventionally magnetic elements with either a partially filled *d* band or *f* band are present.

Several theoretical approaches have been proposed to understand the high-temperature ferromagnetism.[1,3–5] For some of them, the correlation between the electronic band structure and magnetic properties is crucial. For example, ferromagnetism has been attributed to a peculiar property of a dilute electron gas within the framework of carriers in the conduction band induced by La doping in an otherwise semimetallic system.[6] Alternatively, it has also been suggested that the ferromagnetism may be associated with a doping-induced departure from an excitonic ground state.[3,5,7] For other explanations, the role of variation in chemical composition (Ca or B vacancies),[2,8,9] defects,[8] or impurities[10] has been emphasized.

Measurements have also shown that both stoichiometric CaB_6 and nonstoichiometric $Ca_{1-\delta}B_6$ have large thermoelectric power at room temperature.[11,12] The high negative values of the thermoelectric power for both materials indicate a low concentration of itinerant *n*-type charge carriers.[11] La- (or Y-) doped CaB_6 is also predicted to be a candidate for an *n*-type thermoelectric conversion material.[13] The understanding of the mechanisms involved in *n*-type thermoelectric conversion depends on a detailed knowledge of the electronic structure, in particular the nature of the unoccupied density of states (DOS) at the bottom of the conduction band.

The electronic structure of CaB_6 has been studied both experimentally[14,15] and theoretically.[16–19] Most studies have concentrated on the occupied states and the possible existence of a semiconducting gap at the Fermi level. Electronic structure calculations in the local density approximation (LDA) for CaB_6 yield a semimetallic ground state, with a small overlap between the valence band and the conduction band at the *X* point of the Brillouin zone.[16,17] A more sophisticated calculation of the single-particle excitation spectrum of CaB_6 employing the *GW* approximations,[20] based on the pseudopotential plane wave method, suggests that this compound is a semiconductor, with a rather large band gap of 0.8 eV.[18] However, a more recent *GW* approximation calculation based on the linear-muffin-tin-orbital (LMTO) method by Kino *et al.* shows that electron correlation does not open a band gap.[19] X-ray photoemission spectroscopy has been used as a probe of the density of states of the occupied valence band, while x-ray absorption spectroscopy (XAS) has been used as a probe of the unoccupied conduction band states, both measurements suggesting that stoichiometric CaB_6 is a semiconductor.[14] The band structure determined by angular resolved photoemission spectroscopy (ARPES) shows a 1 eV energy gap at the *X* point.[14,15] However, the x-ray absorption data also indicate that the surface of the crystals used in these studies may have been oxidized.[14]

Determination of the intrinsic electronic structure of CaB_6 is experimentally challenging because of possible inhomogeneities in the CaB_6 system, particularly in the near surface layer.[10,21] Since both photoemission and x-ray absorption spectroscopies are broad area techniques and probe only the near surface region of samples, alternative bulk-sensitive

probes for the intrinsic electronic structure of these materials are highly desirable. As a part of a wide-ranging research program investigating the origin of its weak ferromagnetism, we have employed EELS to investigate the chemical and electronic structural change in CaB_6. The B K edge is an ideal signal for EELS study, as good signal-to-noise ratios can be easily achieved on account of the high excitation cross section associated with the low energy loss involved (188 eV at the B 1s absorption threshold). For our experimental conditions, where small-angle scattering dominates, the information obtained with EELS is equivalent to that from XAS, apart from an angular integration factor. With high-energy electrons propagating through the whole thickness of the thin film sample, EELS is, however, more sensitive to the electronic structure of the bulk material. In conjunction with high-resolution transmission electron microscopy (HRTEM), EELS can also reveal spatially resolved information about chemical composition and electronic structure on a nanometer scale, making it a suitable technique to study CaB_6 samples that also contain impurity phases.

Although the B 1s absorption edges have not been as extensively studied as C 1s absorption signals, the fine structures known for several materials show that the B 1s absorption edges are sensitive to the environment and bonding of the excited atom.[22–29] In order to correlate the fine structure in the B 1s core-level absorption edge with the electronic structure in CaB_6, we have also carried out simulation of EELS data. A comparison between the experimental and theoretical spectra shows excellent overall agreement, revealing the effects of Ca hybridization on electron energy-loss near-edge fine structure (ELNES). The transition into the states near the Fermi level has also been investigated carefully. A discrepancy between the theory and experiments indicates the inadequacy of current single-particle EELS calculations, as well as the need for better high-resolution experimental data at the Fermi level.

II. EXPERIMENT

CaB_6 powder samples were prepared according to the following boron-reduction solid-state reaction:

$$CaO + 7B \rightarrow CaB_6 + BO.$$

The synthesis was carried out using spectra-pure CaO and B at 1450 °C under an Ar atmosphere. X-ray diffraction showed that the resulting compound was single phase, and measurement by a vibration magnetometer at room temperature showed that the compound was ferromagnetic, with a saturation moment of 2.29 emu/mol. Sintered samples were either ion beam thinned or simply crushed between glass plates to produce electron beam transparent specimens.

Electron energy-loss spectroscopy was performed in a JEOL 2010F transmission electron microscope operating at 200 kV with a thermally assisted field-emission gun. The B 1 s core-level absorption spectra were obtained with an energy dispersion of 0.3 eV per channel, with a nearly parallel electron beam, with a spectrometer collection semiangle of 3.4 mrad, and with the microscope in diffraction mode. Chemical analysis by energy dispersive spectrometry confirmed that the investigated grains were CaB_6. The energy resolution (measured as the full width at half maximum of the zero-loss peak) was typically 1.6–1.8 eV. The pre-edge background was subtracted using a standard power-law extrapolation[30] method. Spectra were deconvolved of multiple scattering effects using the Fourier-ratio method[30], with the low-loss contribution measured separately.

III. THEORETICAL METHOD

A. Single-particle electronic structure calculation

The B 1 s absorption calculation was based on a plane-wave pseudopotential method in the framework of density functional theory[31] (DFT) using a generalized gradient approximation (GGA). The Vanderbilt ultra-soft ionic pseudopotential[32] was employed for the representation of the atomic cores. The gradient-corrected functional [Perdew-Wang 1991 (PW91)] exchange-correlation approximation[33] was employed, both in the pseudopotential generation and in the self-consistent band-structure calculations. The calculation was performed using the experimental lattice constant (4.146 Å).[16] A plane-wave cutoff of 450 eV was used. The Brillouin zone integration was carried out on an equivalent Monkhorst-Pack k-point mesh[34] with 216 k points used in the first Brillouin zone for the ground state calculation. The local basis consisted of the 2s, 2p orbitals for B, and of the 3s, 3p, 3d, and 4s orbitals for the Ca atoms.

The total density of states (TDOS) was obtained directly from the band structure of the self-consistent calculation. The band structure calculation was carried out non-self-consistently for each band line, i.e., a Harris-type calculation, where the electron density is not updated, using the self-consistent electron density as an input.

B. Near-edge structure calculation

The electron energy-loss cross section is given by the Fermi golden rule[30]

$$\frac{d^2I}{d\Omega dE} = \sum_f \frac{4\gamma^2}{a_0^2} \left| \frac{\langle f|\exp(i\vec{q}\cdot\vec{r})|i\rangle}{q^2} \right|^2 \delta(E_f - E_i - E), \quad (1)$$

where $\vec{q}$ is the wave vector of the momentum transfer during an electron-energy loss event, a_0 is the Bohr atomic radius, γ is the relativistic correction factor, and $|i\rangle$ and $\langle f|$ are the initial and final states respectively, of the excited electron in the sample.

In the single-particle calculation, all electrons (taking the total number to be N) are treated as independent, with the mutual interactions being taken into account through a self-consistent mean-field potential. Thus the total wave function can be written as a product of N single-particle wave functions. The initial and the final states involved in a single-particle excitation (such as for a core electron excitation) can then be written as

$$|i\rangle = |N_{th}\rangle|N-1\rangle, \quad |f\rangle = |N_{th}^*\rangle|N-1\rangle, \quad (2)$$

where the Nth electron is directly excited by the external perturbation associated by the passage of fast electrons. The

initial and final states in Eq. (1) can then be replaced by the initial and final states, respectively, of the excited (*N*th) electron, as provided by the single-particle calculation.

Strictly speaking, the one-electron eigenvalues derived from the Kohn-Sham density functional theory cannot formally be interpreted as quasiparticle energies. In practice, however, the band structures resulting from such calculations have been found to be very useful in interpreting the electron spectroscopy of solids.[35] We have adopted a similar computational approach, bearing in mind this limitation, particularly with regard to the inability to fully take into account the many-body interactions.

For small-angle scattering, the dipole transition dominates and the transition matrix can be approximated as

$$\langle f|\exp(i\vec{q}\cdot\vec{r}|i\rangle \approx i\langle f|\vec{q}\cdot\vec{r}|i\rangle. \quad (3)$$

As we are dealing with an inner-shell excitation, the initial state of the excited electron can be approximated by the atomic equivalents with well-defined orbital angular momentum quantum numbers. The angular integrals in the matrix element calculation then lead to the dipole selection rule $\Delta l = \pm 1$ for the accessible final state. The radial integrals are determined by the radial overlap between the core and the conduction-band wave functions. The core-level spectra are normally considered therefore to be proportional to the site- and angular-momentum-projected density of the final states of the excited electron. In the present work, we have used the local partial density of states (PDOS) of the pseudopotential single-particle calculation to interpret the near-edge fine structure for CaB_6. The radial projections were approximated as $\langle \Psi|S|\phi_{\text{atom}}\rangle$; thus, one-electron wave functions were projected onto the core atomic orbital (ϕ_{atom}) at the site of the excited atom. Note that S is a Hermitian overlap operator, taking care of the ultrasoft nature of the pseudopotential employed.[32] We have mimicked the effect of the radial matrix element by choosing the projection-sphere radius S_α be similar to the radial extension of the core-state wave function involved.[36] Taillefumier *et al.*[37] calculated the Si *d* and O *p* DOS using an integration sphere of 0.4 Å radius; the resulting PDOS's were similar to the result from a direct matrix element calculation. In our case, projected-sphere radii of 0.13 Å, 0.26 Å, 0.53 Å, and 1.15 Å have been tested to check the influence of the choice of cutoff radius on the projected local DOS. All of these projected-sphere radii are larger than the probable radius of the B 1*s* core orbital of 0.11 Å. The value of the radial function of the B 1*s* core state decreases to one-tenth of the maximum value at 0.59 Å, and to 1% at 0.94 Å. The projected local DOS results were similar, except for the case of 1.15 Å, indicating that the calculated PDOS is insensitive to the size of the cutoff radius when this radius is small. Our calculation, employing a 1.15 Å cutoff radius, produces a reasonable number of the total occupied electrons and was used to produce the total DOS and the partial DOS. However, the integration volume obtained using this value is much larger than the spatial extent of the B 1*s* orbital, and the corresponding cross-section calculation shows an overestimation of absorption intensities for the low excitation energy compared to the results for 0.13 Å, 0.26 Å, and 0.53 Å. In the following results, the projection radius for the B 1*s* core-level spectroscopy calculation was chosen as 0.26 Å. The energy dependence of the radial matrix element is ignored in our approach, but it usually has only a very small effect.[37].

C. Core-hole effect

The core-hole effect[35–40] arises because an additional attractive potential emerges during the excitation process, due to an inadequate screening of the nuclear charge after the removal of an excited electron from the core level. To model the excited atom in which the hole is localized, a pseudopotential for excited states was specially constructed by reducing the occupation of the core level (the 1*s* state for the B 1*s* absorption calculation) of the reference configuration by one, i.e., using a $1s^1 2s^2 2p^2$ atomic reference configuration for boron. To minimize the mutual interaction of excited centers in the nearest cells, a supercell containing $2\times2\times2$ primitive cells was constructed in which only one atom was excited. The minimum distance between neighboring excited atoms was 0.83 nm; this was found to be large enough to avoid interactions between excited centers located in neighboring supercells. A plane-wave cutoff of 360 eV was used. This value is slightly lower than that used for the ground state calculation, in order to reduce the calculation overhead. The effect on convergence of PDOS features has been carefully tested. For the supercell calculation, 64 *k* points were used for the first Brillion zone.

IV. RESULTS

A. Electronic structure of CaB_6

The calculated band structure of CaB_6 is shown in Fig. 1(b), and is in overall agreement with other calculated results.[16–19] To facilitate understanding of the overall features of the band structure, we have also plotted the corresponding band structure for a "fictitious" B_6 cluster framework crystal (obtained with all the Ca atoms removed from the CaB_6 crystal) and for the isostructural compound LaB_6. The dominant features of the band structure, particularly for the valence band, can be attributed to the electronic states of the three-dimensionally interconnected B_6 clusters. The main effect of metal atom additions (Ca and La) is to shift the Fermi level upwards in accordance with the electron counting rule, where each Ca (La) atom donates 2 (3) electrons to the valence band. However, the dispersion of the "B_6"-related band also changes significantly in addition to the presence of additional levels in the conduction band due to Ca or La atoms. Our DFT-GGA calculation shows that the valence band and the conduction band are just touching at the *X* point at the Fermi level. In comparison, DFT-LDA results[16,17] show a slight band overlap. A *GW*-approximated band structure starting from a LDA calculation performed with a plane wave basis and using norm-conserving pseudopotentials has suggested that CaB_6 is a semiconductor with a band gap of 0.8 eV.[18] Another *GW* calculation using LMTO wave functions as inputs, however, shows no such gap.[19] These conflicting results indicate that the details of the band structure near the Fermi level are clearly very sensitive to the way that

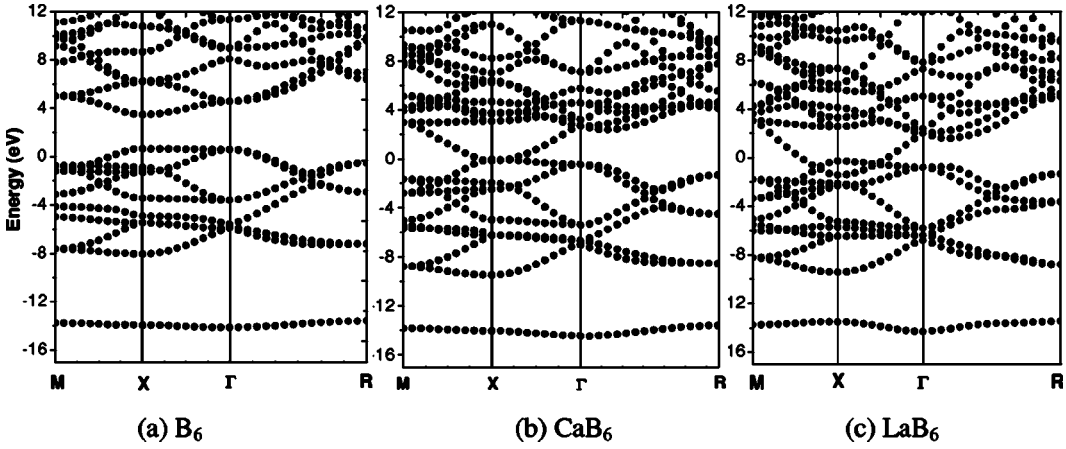

FIG. 1. The single-particle electronic band structure for a fictitious octahedron B_6 crystal (a), CaB_6 (b), and LaB_6 (c) calculated using the pseudopotential plane-wave method.

the many-body correction[41] is introduced. Nevertheless, throughout the Brillouin zone, the band dispersion in our DFT-GGA calculation is similar to that of the reported DFT-LDA and *GW* data. Thus, the electronic state relative to ground state properties may still be interpreted by our DFT-GGA pseudopotential plane wave calculation, particularly for states away from the Fermi levels, even though the band gap as a many-body property may not be well reproduced in the present single-particle ground state calculation.

The total and partial DOS profiles of CaB_6 are shown in Fig. 2. As we are primarily interested in the fine structure of the B 1*s* core-level absorption spectrum, we have plotted the DOS profile with a 0.4 eV broadening, in order to obtain an overview. The total DOS is given in panel (a), showing that the Fermi level is located in a region of low density of states, with the additional electrons occupying the strongly dispersed conduction band (see Fig. 1). The valence bands are mainly composed of the boron orbitals, as shown in panel (b) for boron *s* and in panel (c) for boron *p* symmetry-projected DOS. The nature of the site and angular-momentum projections is different in the conduction band region, where a prominent peak in the calcium 3*d* PDOS exists as shown in panel (f). The Ca *s* and *p* PDOS do not make any important contribution over the energy range concerned; to show them, they have been enlarged 30 times in panels (d) and (e). The valence states with Ca *p*-like PDOS are mainly localized at a deep energy range, about 22 eV below the Fermi level (2*p* semicore state), and a few eV above the Fermi level. A comparison with the TDOS of the fictitious "B_6" compound is shown in Fig. 3, where the valence band DOS resembles that of CaB_6, in agreement with our analysis of Fig. 1. This similarity shows that the Ca atom plays mainly an ionic role, with charge transfer from its *s*, *p*, and *d* states. However, hybridization of boron *p* orbitals with its empty 3*d* states does have some influence on the structure of the density of states near the Fermi level, as the mixing of the two are significant over this energy range. This behavior is different from other semimetallic systems where the states near the Fermi level are dominated by one angular symmetry component (e.g., p_z in graphite), and may be responsible for the observed sensitivity of the calculations to the different methods of incorporating the many-body perturbations[19].

In discussing the possible intrinsic mechanisms of ferromagnetism in CaB_6, it is important to know the Fermi level

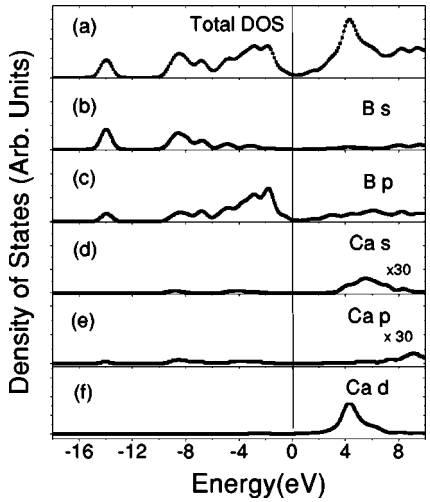

FIG. 2. The total density of states (TDOS) curve for CaB_6 (a) and the symmetry-projected density of states for the boron atomic site (b) and (c), and for the calcium atomic site (d)–(f).

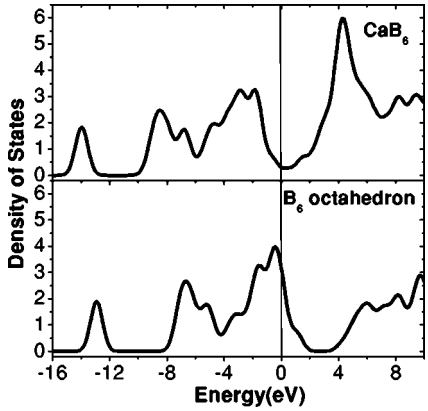

FIG. 3. Total density of states (TDOS) for the fictitious B_6 octahedral crystal (lower panel) compared with that for CaB_6 (upper panel).

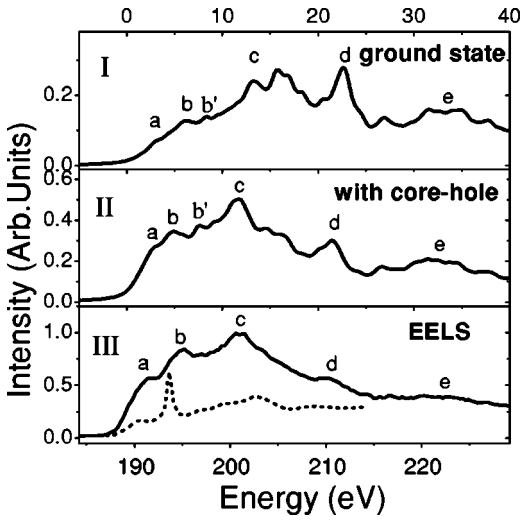

FIG. 4. Calculated ELNES without inclusion (panel I), and with inclusion (panel II) of the core-hole effect; both are convolved with a Lorentz function of a width of 1.3 eV. The experimental ELNES (panel III) has a width mainly caused by a combination of the instrumental resolution limit (1.6–1.8 eV) and lifetime broadening. The XAS-TEY spectrum from Ref. 14 is reproduced in panel III (short dashed line).

shift associated with electron or hole doping of the CaB_6 parent compounds either from La doping[1] or as the result of a Ca deficiency.[2] This has been simulated using a supercell model with 56 atoms (including 8 Ca atoms). A 0.45 eV shift can be identified after removing one electron, translating into a 3.2 eV shift per electron per primitive cell. For example, a 1% Ca deficiency in the sample could induce a shift of 0.06 eV at the Fermi level.

B. Simulation of B *K*-edge electron energy-loss spectrum

Figure 4 compares the experimental and calculated ELNES of the B *K*-edges of CaB_6, for calculations using the ground state information only [Fig. 4(I)], and including the core-hole effects [Fig. 4(II)]. To facilitate comparison with the experimental spectrum [Fig. 4(III)], the calculated spectra have been convolved with a Lorentz function of a fixed width of 1.3 eV. This width is chosen so as to avoid showing excessive detail, but that the resolution of the theoretical spectra is still slightly better than the experimental result, such that no fine feature may be overlooked. In practice, the lifetime broadening may vary with the excitation energy;[42,43] this modification is not included in Fig. 4. We have labeled the main peaks alphabetically, as shown in Fig. 4. The core-hole calculation and experimental spectra are aligned according to the energies of peaks labeled *c* and *d*. The theoretical calculated spectra with and without core-hole effects, Figs. 4(I) and 4(II), are aligned with respect to the Fermi level, which was set to zero (shown on the upper energy scale of the figure). It is clear that the presence of the core hole induces a general transfer of spectral-weight from the high-loss region to the absorption threshold. However, no additional peak features are induced. The relative intensities of the peaks labeled *a* and *b* are enhanced, and have a decreased separation. The dominant peak *c* in the spectra is modified both in its energy position and in its shape by the core-hole interaction. At high energies, the width of the peak *d* is only slightly adjusted, and the shape of the peak *e* remains unchanged.

C. Experimental result and comparison

The experimental spectrum in Fig. 4(III) is taken from an area within a single CaB_6 grain to minimize the contribution from intergranular phases with different chemistry (a detailed microstructural investigation will be reported elsewhere). The shape of the spectrum is very similar to that reported by Hoffmann *et al.*[25] A careful examination of spectra taken from different regions of the specimen shows, however, that the relative intensity of the experimental peak *b* sometimes varies. For previously published XAS experimental spectra[14] [reproduced as a dashed line in Fig. 4(III)] obtained using the total electron yield method (TEY), a sharp peak appears at a similar energy. This peak has been attributed to surface boron oxide.[14] This shows that although XAS is more bulk-sensitive than photoemission experiments, the influence of surface contamination and from intergranular phases can still have a significant effect on x-ray absorption spectra taken from a large surface area. The close resemblance between the energy position of the sharp peak in the TEY spectra and of the intensity-varying peak *b* suggests that these peaks may be of the same origin. The comparatively weaker signal seen in the EELS data suggests that this peak is a surface effect. Comparison with the B *K*-edge spectra of boron oxide[44] suggests that it may be caused by an oxidized phase either in the surface or at the intergranular layer. Overall, we believe that the high energy EELS result is much more representative of the bulk property of CaB_6 than data obtained using the XAS-TEY method.

The ELNES data calculated including the core-hole effect give a better overall agreement with the experimental ELNES data than the simulation using the ground state calculation only [Figs. 4(I) and 4(II)]. Both calculations correctly reproduce the five main peaks found in the experimental spectrum, but the relative intensities from the core-hole simulation are in particularly good agreement with the experiments. The main discrepancy between the core-hole simulation and the experimental result is the splitting of peak *b* in the simulated result in the energy region corresponding to peak *b* in the experimental spectrum. This discrepancy may be due to the possible presence of the unavoidable surface oxide layer. Another difference between the simulated and experimental data is the apparent "shrinking" in the energy scale near the Fermi level, i.e., the energy separation between peak *a* and peak *c*. The distance in the core-hole calculation result (~9 eV) is smaller than that found in the experimental spectrum (~9.6 eV). A detailed comparison of the relative peak positions in Figs. 4(I) and 4(II) reveals that inclusion of core-hole effects results in a downshift of all peaks to lower energies with respect to the Fermi level, though the amount of shift is different for each peak, being most significant for peaks within 25 eV from the Fermi level. A similar difference in the apparent energy scaling can also

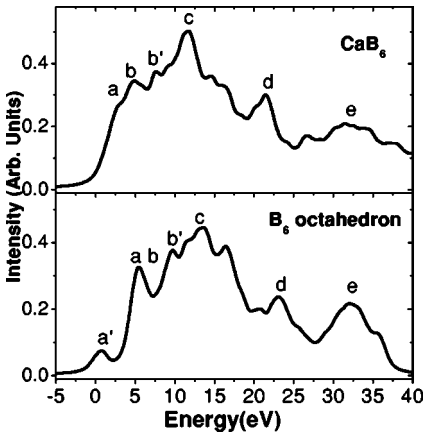

FIG. 5. The simulated B *K*-edge ELNES for the fictitious B_6 octahedron (lower panel) compared with that for CaB_6 (upper panel).

be found in the B *K*-edge simulation of cubic BN.[39]

Overall, the core-hole calculation shows a good one-to-one correspondence between ground state information, such as the PDOS, and the spectral features in the B *K*-edge spectrum. It is still possible therefore to study the nature of the unoccupied states in CaB_6 using B 1*s* absorption spectroscopy, as long as the influence of the core hole is properly taken into account.

V. DISCUSSION

A. Spectral signature of Ca-B hybridization

The comparison of the electronic density of states of CaB_6 and B_6 (Fig. 3) reveals a relatively large difference in their unoccupied density of states. The biggest difference is mainly located at 4 eV above the Fermi level and is attributed to Ca *d* orbitals in CaB_6. There is a corresponding peak in the B 2*p* symmetry-projected DOS, indicating that there exists a certain degree of hybridization. This peak is labeled as *b* in the ground state ELNES simulation results (Fig. 4). This feature is also observed in the calculation taking into account the core-hole effect. Thus, we can identify the spectral feature *b* in the simulation as a signature of Ca-B hybridization. The difference in the nature of the density of states at the bottom of the conduction band in the two compounds demonstrates that the bottom of the conduction band in CaB_6 is quite complex, involving hybridization of both B and Ca orbitals. This also means that one cannot strictly interpret the spectral change in $Ca_{1-\delta}B_6$ using a rigid band approach.

Given the importance of the core-hole effect in modifying the appearance of the B 1*s* core-level spectra in CaB_6 (Fig. 4), we have also simulated the B *K* edge of the fictitious B_6 octahedron, employing the same method used for CaB_6. The result is given in Fig. 5 (lower panel), together with the calculated B *K*-edge spectrum of CaB_6 for easy comparison. Given that this comparison is designed to probe the unoccupied states, it is surprising to see a large similarity in the B 1*s* core-level excitation between CaB_6 and "B_6," as the Ca *d* orbitals make a strong contribution in CaB_6 and as this contribution is absent in B_6. This similarity means that hybridization between Ca and B orbitals is not very strong. Careful analysis shows two distinct differences. A clear difference near the absorption edge can be found. The presence of a distinct pre-edge peak *a* in the spectrum for the "B_6" crystal is the result of the Fermi level shifting into the top of the valence band, which has a high density of states energy region with a major contribution from the boron *p*-symmetry states. The other difference is the absence of peak *b* for the fictitious B_6 structure. Coupled with the fact that Ca *d* components make a bigger contribution to the total density of states for the same energy region, this reinforces our conclusion that peak *b* found in the calculated CaB_6 absorption spectrum is due to hybridization of B *p*-symmetry states with the above-mentioned Ca *d* components. Thus, feature *b* is intrinsically related to the presence of Ca in the compounds.

B. Fine structure at the absorption threshold

So far, we have shown that an *ab initio* calculation for the B 1*s* absorption spectrum can give a reasonably good agreement with the experimental spectra for an energy resolution of the order of 1 eV. For many core-level absorption processes, this resolution is adequate, as the spectral resolution is fundamentally limited by the finite lifetime of the core hole produced during the excitation process. However, for light elements such as boron, the core-hole lifetime can be very long,[22,23] allowing us to study the electronic structure in much finer detail. In this study, we are also interested in the electronic states near the Fermi level because they figure prominently in the discussion of possible mechanisms for intrinsic ferromagnetism[1,4,5] as well as for thermoelectric effects.[11–13] Until now, these states have been studied by photoemission experiments for the occupied states, and by XAS for the unoccupied states. Core-level absorption spectroscopy using EELS is potentially a more bulk-sensitive technique. Our experimental electron energy-loss data lack, however, the necessary resolution for such studies. For the time being, we therefore compare our theoretically derived results with the currently available x-ray absorption data. XAS data for CaB_6, collected using the TEY method, are known to be very surface sensitive and suffer from a large contribution from surface oxides. For our comparison, we have instead used XAS data collected using a partial fluorescence yield (PFY) method,[14] in which the signal is generated over relatively large depths within the sample, and hence is relatively less surface sensitive. These data are reproduced in Fig. 6(a) for easier comparison with our calculated result near the Fermi level. To account for the fine structure revealed by the high-resolution PFY data, the calculation is broadened only to 0.2 eV for this narrow energy range. Whether this high spectral resolution is necessary for evaluating high excitation features in the absorption spectrum remains an open question for this compound.

In general, we expect the lifetime of the quasiparticles to change with the excitation energy.[42,43] However, the precise energy dependence of this change is usually unknown. Initially we concentrate on the spectral details near the absorption threshold, where we may assume that the change is unimportant. Subsequently, we also try several other

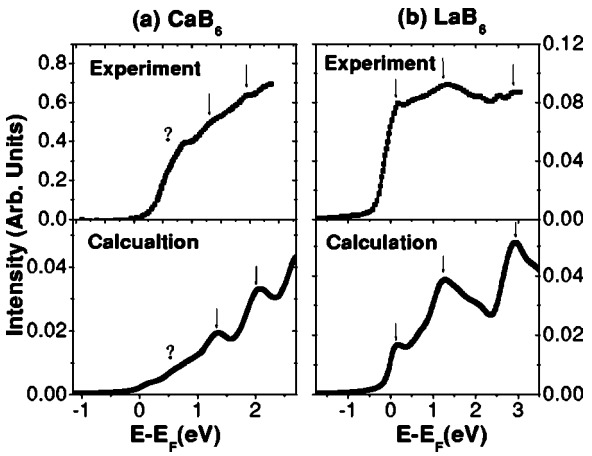

FIG. 6. Comparison of the theoretical and experimental spectra for the near-edge features at the threshold of the B 1*s* absorption for CaB_6 (a) and for LaB_6 (b). The high-resolution experimental spectra are reproduced from Refs. 14 and 45, which were obtained using the partial florescence yield (PFY) method.

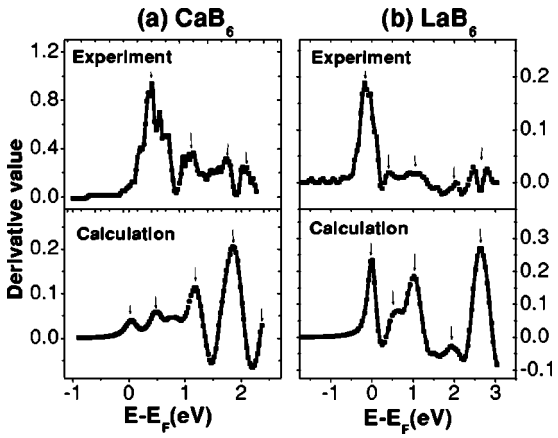

FIG. 7. Comparison of the theoretical and experimental spectra for the near-edge features of the B 1*s* absorption spectra for CaB_6 (a) and for LaB_6 (b). Data are presented in their first derivative forms to highlight the extra feature predicted by the theoretical spectra for CaB_6, and the consistency of the peaks found in the theoretical and experimental spectra for LaB_6.

phenomenological models of the energy dependence of the lifetime over this narrow energy range to test its influence on the spectral appearance.

Although the theoretical spectrum obtained using the single-particle core-hole calculation fits the experimental result reasonably well over a wide energy region at an energy resolution of the order of 1 eV, the comparison between the calculated and experimental results in Fig. 6(a) suggests that the present spectral simulation does not reproduce the experimental spectral features near the Fermi level at the finer 0.2 eV scale. The PFY spectrum for CaB_6 shows a weak steplike threshold onset, whereas the single-particle calculation shows a gradual rise from the Fermi level. The theoretical and experimental spectra have been aligned according to the peaks indicated in Fig. 6(a). This alignment may not be entirely justified, because it is hard to identify a one-to-one correspondence for the features in the two spectra. Nevertheless, the discrepancy in spectral shape is independent of the peak identification.

C. Comparison with LaB_6

To investigate the suitability of our current calculation method for studying the band structure at the Fermi level, we have also used an identical procedure to calculate the boron 1*s* absorption spectrum for LaB_6. The PFY spectrum[45] of LaB_6 is reproduced for easier comparison with our calculated result in Fig. 6(b). In contrast to the case for CaB_6, there is a clear one-to-one correspondence of the spectra features over an energy range of 3 eV at a resolution of 0.2 eV. This correspondence shows that the overall features of the absorption edge in the metallic LaB_6 system can be reasonably well described by our *ab initio* single-particle calculation, even at this fine energy scale.

The differences between the experimental and theoretical results in Fig. 6 can be seen more clearly by looking at the derivatives of the spectra, as shown in Figs. 7(a) and 7(b). In contrast to the consistency in peak position and number for LaB_6, a comparison between the experimental and theoretical derivatives of the x-ray absorption spectra reveals an additional peak near the Fermi level in the theoretical spectrum for CaB_6, which is absent in the experimental spectra.

In both the CaB_6 and LaB_6 cases, the relative intensities of the experimental peaks are not particularly well reproduced by the simulations. One possible reason may be experimental, as the PFY detection method of soft-x-ray absorption suffers from possible saturation effects caused by self-absorption of the emerging x-ray fluorescence. This can cause a nonlinearity in the detection of the intense peaks in the absorption spectra (the so-called saturation effect[46,47]). In addition to possible false peaks due to the experimental noise, and to suppression of high intensity peaks resulting from possible saturation in fluorescence measurements, another important reason for the difference may be that the energy-dependent lifetime effects of the inelastic photoexcited electrons vary dramatically near the threshold and that such effects cannot reproduced as the many-body interactions are not entirely included in the calculation.[48]

D. Modeling the energy dependence of the core-hole lifetime

The actual lifetimes are the result of a delicate balance between localization, density of states, screening, and Fermi-surface topology.[43] So far, the broadening width used for the theoretical spectra in Figs. 6(a) and 6(b) is assumed to be constant over the energy range shown. We have attempted to estimate the effect of the energy-dependent lifetime broadening on the change in relative peak intensity by looking at the sensitivity of the spectral change for various assumed energy dependencies for the excited electrons. The effect of different energy dependencies is shown in Fig. 8. We found that while the peak intensity does change, the peak positions and numbers in the derivative spectra remain unchanged. We conclude therefore that although energy dependent lifetime broadening is an important factor for simulation of high-

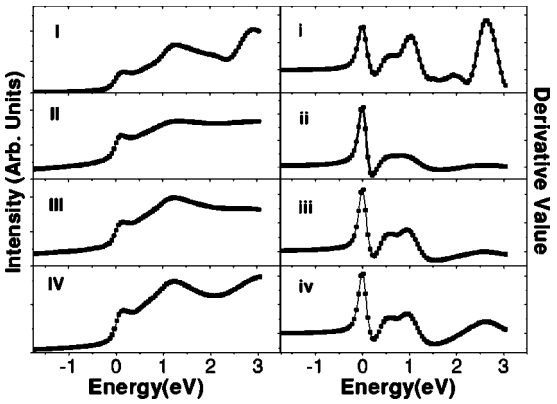

FIG. 8. The effect of different energy dependences of the lifetime effect on the appearance of the near-edge feature at the B 1*s* absorption threshold of the compound LaB_6: (I) a constant 0.2 eV, (II) $0.15+0.5E+0.05E^2$, (III) $0.15+0.2E^2$, (IV) $0.15+0.2E^2$ for $E<1.0$ eV and 1.0 eV for the higher excitation energy. Also shown are the corresponding spectra in their derivative forms.

resolution spectra, it cannot explain the main discrepancy for CaB_6 between the high-resolution simulation and the XAS-PFY data.

Alternatively, the discrepancy between the experimental spectrum and the single-particle core-hole calculation result for CaB_6 may reflect the importance of the many-body interactions, which are not fully taken into account in the present simulation. This may be related to the controversy over the existence and the nature of an energy gap in the electronic states.[14,16,18,19] We hope that our work will stimulate more detailed experimental and theoretical work to settle this question definitively.

VI. CONCLUSION

Experimental EELS investigation of the B 1*s* core-level spectroscopy has revealed inconsistencies, which may be due to the ubiquitous oxide at both surfaces and interfaces of CaB_6 grains. The intrinsic part of the B 1*s* core level spectrum is found to be in excellent overall agreement with the *ab initio* theoretical simulation that takes into account the core-hole effect. By studying the ground state electronic structure, we can identify a specific feature associated with boron *p* orbitals hybridized with the Ca *d* orbitals. This interpretation is confirmed by the results of a simulation of the fictitious "B_6" compound. However, comparison of the high-resolution simulated spectra and the high-resolution x-ray absorption spectra for states near the Fermi level shows a significant discrepancy. This may point to the importance of correctly accounting for the nature of the many-body interactions for states at the Fermi level in CaB_6. The results of the investigation highlight the need for better experimental results that can truly reflect bulk intrinsic properties of this material.

ACKNOWLEDGMENTS

The simulation work was mainly carried out using the computer code DACAPO of the CAMP Open Software Project, Denmark. The research is supported by the National Key Research and Development Project for Basic Research (Grant No. 2002CB613500 from the Ministry of Science and Technology), the National Natural Science Foundation of China, the Changjiang Scholar Program of Ministry of Education and the 985 funding of Tsinghua University. We thank Professor A. Godfrey for a careful reading of the text.

*Author to whom correspondence should be addressed. Electronic address: yuanjun@tsinghua.edu.cn

[1] D. P. Young, D. Hall, M. E. Torelli, Z. Fisk, J. D. Thomson, H. R. Ott, S. B. Oseroff, R. G. Goodrich, and R. Zysler, Nature (London) **397**, 412 (1999).
[2] T. Moriwaka, T. Nishioka, and N. K. Sato, J. Phys. Soc. Jpn. **70**, 341 (2001).
[3] S. Murakami, R. Shindou, N. Nagaosa, and A. S. Mishchenko, Phys. Rev. Lett. **88**, 126404 (2002).
[4] C. Hotta, H. Fukuyama, and M. Ogata, Phys. Rev. B **65**, 184421 (2002).
[5] M. E. Zhitomirsky, T. M. Rice, and V. I. Anisimov, Nature (London) **402**, 251 (1999).
[6] D. Ceperley, Nature (London) **397**, 386 (1999).
[7] M. E. Zhitomirsky and T. M. Rice, Phys. Rev. B **62**, 1492 (2000).
[8] S. E. Lofland, B. Seaman, K. V. Ramanujachary, N. Hur, and S. W. Cheong, Phys. Rev. B **67**, 020410(R) (2003).
[9] R. Monnier and B. Delley, Phys. Rev. Lett. **87**, 157204 (2001).
[10] T. Mori and S. Otani, Solid State Commun. **123**, 287 (2002).
[11] K. Giannò, A. V. Sologubenko, H. R. Ott, A. D. Bianchi, and Z. Fisk, J. Phys.: Condens. Matter **14**, 1035 (2002).
[12] K. Giannò, A. V. Sologubenko, H. R. Ott, A. D. Bianchi, and Z. Fisk, J. Phys.: Condens. Matter **15**, 6739 (2003).
[13] Y. Imai, M. Mukaida, M. Ueda, and A. Watanabe, Intermetallics **9**, 721 (2001).
[14] J. D. Denlinger, J. A. Clack, J. W. Allen, G.-H Gweon, D. M. Poirier, C. G. Olson, J. L. Sarrao, A. D. Bianchi, and Z. Fisk, Phys. Rev. Lett. **89**, 157601 (2002).
[15] S. Souma, H. Komatsu, T. Takahashi, R. Kaji, T. Sasaki, Y. Yokoo, and J. Akimitsu, Phys. Rev. Lett. **90**, 027202 (2003).
[16] S. Massidda, A. Continenza, T. M. de Pascale, and R. Monnier, Z. Phys. B: Condens. Matter **102**, 83 (1997).
[17] S. Massidda, R. Monnier, and E. Stoll, Eur. Phys. J. B **17**, 645 (2000).
[18] H. J. Tromp, P. van Gelderen, P. J. Kelly, G. Brocks, and P. A. Bobbert, Phys. Rev. Lett. **87**, 016401 (2001).
[19] H. Kino, F. Aryasetiawan, K. Terakura, and T. Miyake, Phys. Rev. B **66**, 121103 (2002).
[20] L. Hedin, Phys. Rev. **139**, A796 (1965).
[21] C. Meegoda, M. Trenary, T. Mori, and S. Otani, Phys. Rev. B **67**, 172410 (2003).
[22] M. Terauchi, Y. Kawamata, M. Tanaka, M. Takeda, and K. Kimura, J. Solid State Chem. **133**, 156 (1997).
[23] M. Terauchi, Y. Kawamata, M. Tanaka, H. Matsuda, and K.

Kimura, J. Solid State Chem. **133**, 152 (1997).
[24] H. K. Schmid, Microsc. Microanal. Microstruct. **6**, 99 (1995).
[25] K. Hofmann, and R. Gruehn, and B. Albert, Z. Anorg. Allg. Chem. **628**, 2691 (2002).
[26] K. Hofmann and B. Albert, ChemPhysChem **3**, 896 (2002).
[27] K. Lie, R. Hoier, and R. Brydson, Phys. Rev. B **61**, 1786 (2000).
[28] I. Tanaka, H. Araki, M. Yoshiya, T. Mizoguchi, K. Ogasawara, and H. Adachi, Phys. Rev. B **60**, 4944 (1999).
[29] S. Suzuki, M. Tomita, and T. Hayashi, J. Phys. Soc. Jpn. **34**, L191 (1995).
[30] R. Egerton, *Electron Energy Loss Spectroscopy in the Electron Microscope* (Plenum, New York, 1996), p. 269 p. 264 , and p. 227.
[31] M. C. Payne, M. P. Teter, D. C. Allan, T. A. Arias, and D. Joannopoulos, Rev. Mod. Phys. **64**, 1045 (1992).
[32] K. Laasonen, A. Pasquarello, R. Car, C. Lee, and D. Vanderbilt, Phys. Rev. B **47**, 10142 (1993).
[33] J. P. Perdew, J. A. Chevary, S. H. Vosko, K. A. Jackson, M. R. Pederson, D. J. Singh, and C. Fiolhais, Phys. Rev. B **46**, 6671 (1992).
[34] H. J. Monkhorst and J. D. Pack, Phys. Rev. B **13**, 5188 (1976).
[35] P. Rez, J. R. Alvarez, and C. Pickard, Ultramicroscopy **78**, 175 (1999).
[36] C. Elsässer and S. Köstlmeier, Ultramicroscopy **86**, 325 (2001).
[37] M. Taillefumier, D. Cabaret, A.-M. Flank, and F. Mauri, Phys. Rev. B **66**, 195107 (2002).
[38] S. Köstlmeier and C. Elsässer, Phys. Rev. B **60**, 14025 (1999).
[39] D. N. Jayawardane, C. J. Pickard, L. M. Brown, and M. C. Payne, Phys. Rev. B **64**, 115107 (2001).
[40] W.-Y. Ching, S.-D. Mo, and Y. Chen, J. Am. Chem. Soc. **85**, 11 (2002).
[41] M. S. Hybertsen and S. G. Louie, Phys. Rev. B **34**, 5390 (1986).
[42] J. E. Müller, O. Jepsen, and J. W. Wilkins, Solid State Commun. **42**, 365 (1982).
[43] I. Campillo, J. M. Pitarke, A. Rubio, E. Zarate, and P. M. Echenique, Phys. Rev. Lett. **83**, 2230 (1999).
[44] The B *K*-edge x-ray spectra provided by Karine Varlot (Wisconsin, USA) was found in the EELS and x-ray spectrum database http://www.cemes.fr/~eelsdb/.
[45] J. D. Denlinger, J. W. Allen, and Z. Fisk, http://www-als.lbl.gov/als/compendium/Abstract Maneger/uploads/01090.pdf
[46] R. Nakajima, J. Stöhr, and Y. U. Idzerda, Phys. Rev. B **59**, 6421 (1999).
[47] P. Pfalzer, J.-P. Urbach, M. Klemm, S. Horn, M. L. denBoer, A. I. Frenkel, and J. P. Kirkland, Phys. Rev. B **60**, 9335 (1999).
[48] A. Soininen, Ph.D. thesis, University of Helsinki, Finland, (2001).